# The utilization of Fe-doped g-C 3 N 4 in a heterogeneous photo-Fenton-like catalytic system: the effect of different parameters and a system mechanism investigation

Wei Luo, Wenyu Huang, Xiaoqing Feng, Ying Huang, Xiongwei Song, Hongfei Lin, Shuangfei Wang, Gilles Mailhot

# Utilization of Fe doped g-$C_3N_4$ in heterogeneous photo-Fenton-like catalytic system: different parameters effect and system mechanism investigation

Wei Luo[a], Wenyu Huang[a,b,*] , Xiaoqing Feng [a], Ying Huang [a], Xiongwei Song [a], Hongfei Lin[b], Shuangfei Wang[b,c] and Gilles Mailhot[d]

[a] College of Resources, Environment and Materials, Guangxi University, Nanning 530004, PR China

[b] Guangxi Bossco Environmental Protection Technology Co., Ltd, Nanning, 530007, China

[c] Guangxi Key Laboratory of Clean Pulp & Papermaking and Pollution Control, Guangxi University, Nanning 530004, China

[d] Université Clermont Auvergne, CNRS, SIGMA Clermont, Institut de Chimie de Clermont-Ferrand, F-63000 Clermont–Ferrand, France

[*] Corresponding author.

E-mail address: huangwenyu@gxu.edu.cn (Wenyu Huang)

## Abstract

In this study, a series of Fe-doped g-$C_3N_4$ (Fe-$C_3N_4$) was synthesized and characterized by X-ray powder diffraction (XRD), scanning electron microscopy (SEM), Fourier transform infrared (FTIR), X-ray photoelectron spectroscopy (XPS), UV–vis diffuse reflection spectra (UV-vis DRS), and fluorescence spectra (PL). The photocatalytic activity of the synthesized catalyst was investigated on methylene blue (MB) degradation with hydrogen peroxide ($H_2O_2$) assisting. Results showed that the Fe-$C_3N_4$ heterogeneous photo-Fenton-like system showed a good catalytic performance when the pH value varies from 3.0 to 9.0. For the effect of various inorganic anions in the Fe-$C_3N_4$ heterogeneous photo-Fenton-like system, $HCO_3^-$ showed a dual effect on MB degradation. $Cl^-$ and $NO_3^-$ showed an inhibited effect on MB degradation. For the effect of inorganic cations, $Al^{3+}$, $Mg^{2+}$, and $Ca^{2+}$ showed a strong inhibition in MB degradation. The recycling experiment demonstrated that Fe-$C_3N_4$ possesses good reusability and stability. The quenching experiment was carried out and it was found that hydroxyl radical (·OH) was the major active species in the system. Besides, nine intermediates were identified by LC/MS and a possible pathway of MB degradation in the system was proposed. This study could promote the application of the Fe-$C_3N_4$ heterogeneous photo-Fenton-like system in realistic dye wastewater.



**Key words** Fe doped g-$C_3N_4$, $H_2O_2$, Methylene blue, Heterogeneous photo-Fenton-like reaction, Inorganic ions, Degradation pathway


## 1. Introduction

Nowadays, advanced oxidation processes (AOPs) are commonly recognized as potential alternative technologies for the treatment of refractory organic pollutants, because of their simplicity, high efficiency

and easy handling [1-5]. Among various AOPs, visible light-induced heterogeneous photo-Fenton-like process has been taken into account as an effective way for pollutants treatment. Compared with the traditional Fenton and photo-Fenton process in homogeneous system, it showed many advantages, such as efficient mineralization of organic pollutants, lower cost, reuse, good chemical stability and small amounts of iron precipitation [6]. However, the rigorous pH range (acidic or near-neutral conditions), high iron leaching (>2 ppm), fewer iron active sites and low efficiency cycling of $Fe^{3+}/Fe^{2+}$ limited the application of this process [7]. Therefore, exploring a highly efficient and low-cost catalyst for this system is essential.

Polymeric graphitic carbon nitride (g-$C_3N_4$) as a visible-light-driven photocatalyst has been applied worldly in water splitting, organic degradation, and conversion of $CO_2$ [8-10]. However, the rapid charge recombination has limited its application in AOPs[11, 12]. To overcome this drawback, the external element doped and copolymerized are taken into account and proved to be applicable [13-16]. Fe is an environmentally friendly and abundant element in the earth. It has been extensively investigated to improve the photocatalytic performance of g-$C_3N_4$ by element doping way. Meanwhile, it was certified in previous studies that the photocatalytic activity of g-$C_3N_4$ towards dye degradation can be remarkably improved by Fe doping and Fe existed in Fe-$C_3N_4$ by Fe-N ligand [17-20]. Besides, the photo-induced electrons from Fe-$C_3N_4$ can reduce $Fe^{3+}$ to $Fe^{2+}$ under visible light illumination [21]. Thence, Fe-$C_3N_4$ can work as an efficient catalyst in the heterogeneous photo-Fenton-like system. It has been already reported that the Fe-$C_3N_4$ is an efficient catalyst for removal of organic pollutants in photo-Fenton system. Previous studies have focused on the preparation and optimization of Fe-$C_3N_4$ or coupled Fe-$C_3N_4$ material. The influence of reaction parameters especial for various inorganic ions in natural water on activity and the degradation pathway of specific contaminant (MB) in Fe-$C_3N_4$ based photo-Fenton

system have not been systematically studied. It has been already reported that the Fe-$C_3N_4$ is an efficient catalyst for removal of organic pollutants in photo-Fenton system. However, previous studies have focused on the preparation and optimization of Fe-$C_3N_4$ or coupled Fe-$C_3N_4$ material. The influence of reaction parameters especially for various inorganic ions in natural water on activity and the degradation pathway of specific contaminant (MB) in Fe-$C_3N_4$ based photo-Fenton system have not been systematically studied.

In this study, Fe-$C_3N_4$ was reported as an effectual photo-Fenton-like photocatalyst for MB degradation under simulated sunlight. Various Fe-$C_3N_4$ catalysts with different Fe doping amounts were synthesized and characterized. The effect of important parameters including Fe doping amounts, $H_2O_2$ concentration, catalyst dosage, pH, MB concentration, naturally occurring inorganic ions ($Cl^-$, $NO_3^-$, $HCO_3^-$, $Al^{3+}$, $Mg^{2+}$, and $Ca^{2+}$) and the stability of Fe-$C_3N_4$ were investigated. Besides, scavenging tests were conducted to identify the active species for MB degradation in this catalytic process, and coupling with the intermediate determined by LC-MS, a possible degradation pathway of MB was proposed.

## 2. Experimental

### 2.1 Materials

The chemicals were of commercially available analytical grade used as purchased without further purification. Melamine, ferric nitrate ($Fe(NO_3)_3 \cdot 9H_2O_2$), Hydrogen Peroxide ($H_2O_2$, 30%, w/w), sodium hydroxide (NaOH), hydrochloric acid (HCl), tertiary butanol (TBA), p-benzoquinone, sodium chloride (NaCl), sodium bicarbonate ($NaHCO_3$), sodium nitrate ($NaNO_3$), calcium chloride ($CaCl_2$, P96.0%), magnesium chloride ($MgCl_2$, P98.0%), aluminum chloride ($AlCl_3$, P97.0%)， Potassium iodide (KI), and methylene blue (MB) were supplied by Nanning Lantian Experiment Equipment Co., Ltd (Nanning, China).

## 2.2 Synthesis of Fe-$C_3N_4$

The Fe-$C_3N_4$ catalyst was synthesized according to the method reported [22, 23]. Typically, 6 g melamine was dispersed in 30 ml deionized water under stirring magnetically. Then different dosage of ferric nitrate (0.03, 0.06, 0.12, and 0.3 g) was added. The mixture was heated to 100 ℃ to remove the water. The obtained solid product was milled and put into 25 mL crucible, placed into a muffle furnace and heated to 520 ℃ maintaining 2 h. Finally, yellow powder of Fe-$C_3N_4$ was obtained. The products were labeled x wt% Fe-$C_3N_4$, where x was the mass percent of ferric nitrate to melamine. The pristine g-$C_3N_4$ was synthesized by heating melamine directly under the same conditions without ferric nitrate.

## 2.3 Characterization of catalyst

XRD at a 40 KV operating voltage and 300 mA current (DX-2700A) was applied to determine the crystal structure of g-$C_3N_4$ and x wt% Fe-$C_3N_4$. The morphology of all catalysts was characterized by S-3400N scanning electron microscopy. The functional groups and chemical states of C, N and Fe on the catalyst surface were analyzed by Nicolet iS 50 Fourier transform infrared spectroscopy and ESCALAB 250XI+ X-ray photoelectron spectroscopy. UV-vis absorption spectra were investigated by UV-2501 PC to determine the light adsorption region of catalysts. Photoluminescence were investigated by the ZLX-PL-I fluorescence spectrometer to evaluate the reduction of charge carrier recombination of prepared catalysts.

## 2.4 Experimental procedures

MB was chosen as the model compound to evaluate the efficiency of heterogeneous photo-Fenton-like system. Investigation for the degradation of MB was conducted in a 250 mL quartz reactor at room temperature under stirring magnetically. The MB solutions with different concentrations (20, 30, and 40 $mg \cdot L^{-1}$) were prepared. During each experiment, 200 mL MB was placed in the reactor. The initial pH of

111 the MB solution was not adjusted (initial pH of 6.86) or adjusted with 1 M NaOH and HCl solutions. To
112 achieve the adsorption equilibrium, the catalyst was added into the MB solution at the same time with
113 constant stirring for 30 min without light irradiation. After that, $H_2O_2$ was added and the suspension was
114 exposed to a 150 W xenon lamp. At a given time, about 5 ml of the suspension was removed. The
115 suspension was filtered with 0.22 um the filter heading immediately. To investigate the influence of
116 inorganic ions on MB degradation, the altered concentrations of NaCl, $NaNO_3$, $NaHCO_3$, $CaCl_2$, $MgCl_2$,
117 and $AlCl_3$ with were added. To carry out recycling experiment, the Fe-$C_3N_4$ was removed from the
118 solution by centrifugation. Then Fe-$C_3N_4$ was washed, dried and applied in the next experiment without
119 purification.

120 **2.5 Analytical methods**

121 The absorbance of MB solution was obtained by a 722N Vis spectrophotometer at the wavelength
122 of 665 nm. The removal efficiency of MB was calculated by the following equation (1), where $C_0$ and C
123 were the initial concentration of MB and the concentration of MB after irradiation for a given time,
124 respectively.

125 $$\text{Degradation efficiency}(\%) = \frac{C_0 - C}{C_0} * 100 \quad (1)$$

126 The kinetic analysis of MB degradation used the pseudo-first-order rate model by equation (2),
127 where *k* was the pseudo-first-order rate constant.

128 $$\ln\left({}^{C_0}/_{C}\right) = kt + constant \quad (2)$$

129 The reactive species were investigated by trapping experiment. In this section, 2 mM TBA, 2 mM
130 p-benzoquinone and 2 mM KI were used as the quenchers of ·OH, $\cdot O_2^-$ and $h^+$, respectively. The liquid
131 chromatography coupled with tandem mass spectrometer (LC/MS, AGILENT 6460, America) was
132 applied to analyze the reaction intermediates formed from MB degradation. The related test parameters

133 referred to previous report [24].

134

135 ## 3. Results and discussion

136 ### 3.1 Characterization of g-$C_3N_4$ and Fe-$C_3N_4$

137 The morphology and structure of g-$C_3N_4$ and x% Fe-$C_3N_4$ was observed by SEM (Fig. S1). The

138 result revealed a typical layered structure of all prepared samples. The crystal phase structure of g-$C_3N_4$

139 and x wt% Fe-$C_3N_4$ was investigated by XRD as displayed in Fig.1 (a). Two typical peaks were observed

140 obviously in the XRD patterns of all catalysts. The weak peak at 13.2° and 27.4° was the (100) and (002)

141 facet diffraction peak of the g-$C_3N_4$[25]. With the increase of Fe doping, the diffraction peaks intensities of

142 the (002) facets were gradually weakened. This phenomenon indicated the inhibitory effect of Fe species

143 on polymeric condensation and the host-guest interaction [23]. Furthermore, other characteristic peaks of

144 Fe species were not found that may be caused by limited content of doped iron. Therefore, Fe was

145 probably chemically coordinated to the g-$C_3N_4$ structure in the form of Fe-N bonds [26].

146 The chemical composition and structure of pristine g-$C_3N_4$ and x wt% Fe-$C_3N_4$ samples were

147 investigated by the FT-IR spectroscopy. As shown in Fig.1(b), all materials exhibited characteristic peaks

148 near 3000-3300, 1200-1700, 892, and 806 $cm^{-1}$. Pristine g-$C_3N_4$ and x wt% Fe-$C_3N_4$ samples had similar

149 characteristic peak. This result indicated that the Fe-$C_3N_4$ and pristine g-$C_3N_4$ had the same structure.

150 The broad peak between 3000 and 3300 $cm^{-1}$ was indicative of the terminal N-H stretching vibration.

151 The peaks from 1200 to 1700 $cm^{-1}$ due to the characteristic breathing modes of tri-s-triazine rings. The

152 peak at 892 $cm^{-1}$ was assigned to the cross-linked deformation mode of N-H. Additionally, the peak at

153 806 $cm^{-1}$ due to the tri-s-triazine ring breathing vibration [27, 28].

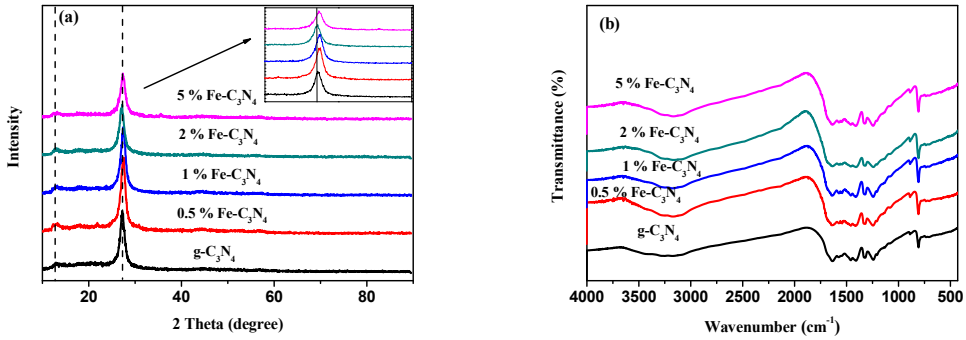


**Fig.1**. XRD patterns **(a)** and FT-IR spectra **(b)** of g-$C_3N_4$ and Fe-$C_3N_4$ samples.

To analyze the elemental composition and the surface states of x wt% Fe-$C_3N_4$, the XPS of 5 wt% Fe-$C_3N_4$ were investigated. As shown in Fig.2(a), four elements were present in the XPS survey spectra of 5% Fe-$C_3N_4$ including C, N, O and Fe. This result was the same as to the EDS analysis that Fe was successfully doped into the structure of 5 wt% Fe-$C_3N_4$ (Fig. S2). The signal of O was ascribed to $O_2$ or $H_2O$ absorbed in the surface of 5 wt% Fe-$C_3N_4$ [29]. The signal of Fe was weak because of the low amount of Fe doping. The C 1s XPS spectra was deconvoluted into two peaks at binding energies of 283.7 and 287.3 eV, as shown in Fig.2(b). The peak at 283.7 eV was the characteristic peak of graphitic carbon C=C and the peak at 287.3 eV was ascribed to the sp2 bonded carbon N-C=C [3, 30]. Fig.2(c) showed that the N 1s XPS spectra was deconvoluted into three peaks at binding energies of 397.9, 399.1, and 400.4 eV, respectively. The main peak at 397.9 eV due to the sp2-bonded N atoms in the triazine rings. The peak at 399.1 eV was attributed to the presence of N-$(C)_3$ or H-N-$(C)_2$. The weaker peak at 400.4 eV was ascribed to the groups of –$NH_2$ or =NH [31]. From Fig. 2(d), the O 1s spectrum exhibits one characteristic peaks at 531.39 eV which was ascribed to surface adsorbed water in the Fe-$C_3N_4$. The Fe-O-Fe and Fe-OH were not found in the Fe-$C_3N_4$ due to the characteristic diffraction peak of Fe-O-Fe and Fe-OH at 529.8 eV. The Fe $2p_{3/2}$ XPS spectrum of 5% Fe-$C_3N_4$ showed a peak centered at 710.4 eV, as shown in Fig.2(e). The binding energy peak of $Fe^{3+}$ at the range from 710.3 to 711.8 eV. Thus, the primary Fe state

on the surface of Fe-$C_3N_4$ was $Fe^{3+}$ [23, 32, 33]. Meanwhile, the binding energy of Fe species stabilized in the g-$C_3N_4$ structure through Fe–N bonds were close to 710.4 eV [19, 34]. Therefore, Fe had been successfully doped into g-$C_3N_4$ and the $Fe^{3+}$ connected to the N atom by Fe–N(III) coordinate bonds.

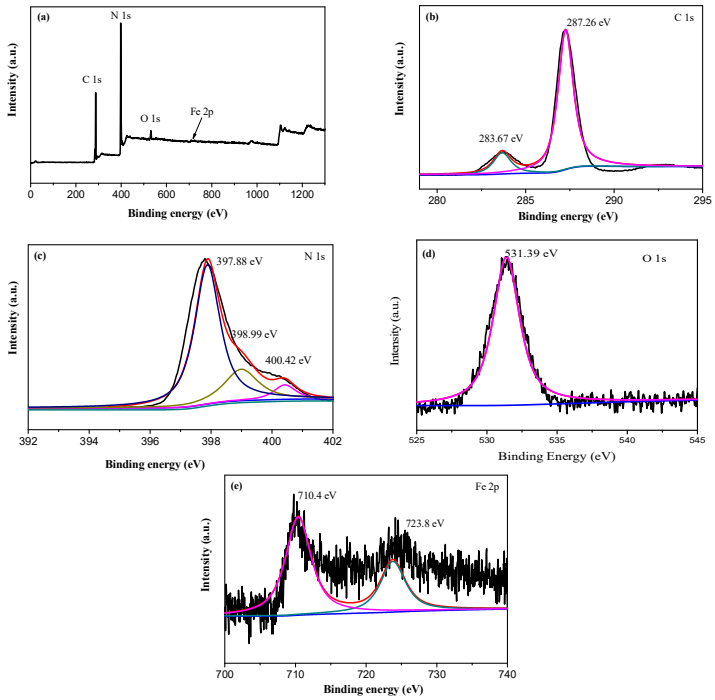


**Fig.2**. XPS spectra of 5 wt% Fe-$C_3N_4$ sample: **(a)** survey scan, **(b)** C 1s, **(c)** N 1s, **(d)** O 1s, and **(e)** Fe 2p.

To estimate the optical properties of all samples, UV-vis DRS was conducted. Fig.3(a) showed the UV-vis DRS spectra of g-$C_3N_4$ and x wt% Fe-$C_3N_4$. Light absorbance of all samples was observed over the range of 250-800 nm. As the amount of iron doping increasing, the absorption range of light gradually increased. This phenomenon indicated that the Fe doping could enhance the light harvesting ability effectively for g-$C_3N_4$. The pristine g-$C_3N_4$ showed an apparent absorption edge at approximately 456 nm. With the increasing of Fe doping, the adsorption edge of Fe-$C_3N_4$ displayed an obvious redshift from 456 to 477 nm. This result was caused by the impurity energy level formation due to Fe doping [22].

The transfer and separation efficiency of photogenerated charge carriers of g-$C_3N_4$ and Fe-$C_3N_4$

were investigated by Photoluminescence (PL) measurements. As shown in Fig.3(b), all samples showed a broad emission peak centered at approximately 438 nm. This result was formed due to the characteristic band-band PL phenomenon of the photoexcited charge carriers for g-$C_3N_4$. The peak intensities of Fe-$C_3N_4$ were far weaker than pristine g-$C_3N_4$ obeying the order of g-$C_3N_4$ > 0.5 % Fe-$C_3N_4$ > 5 % Fe-$C_3N_4$ > 1 % Fe-$C_3N_4$ ≈ 2 % Fe-$C_3N_4$. Thus, the separation and transport efficiency of the photoexcited carriers was enhanced by Fe doping. This result attributed that the Fe doping site in catalyst could trap photogenerated electrons and reduced recombination of photogenerated electron-hole pairs [23]. However, when the doping content of Fe was excessive, a recombination center of electrons and holes may be generated to suppress the separation of photogenerated charges [35].

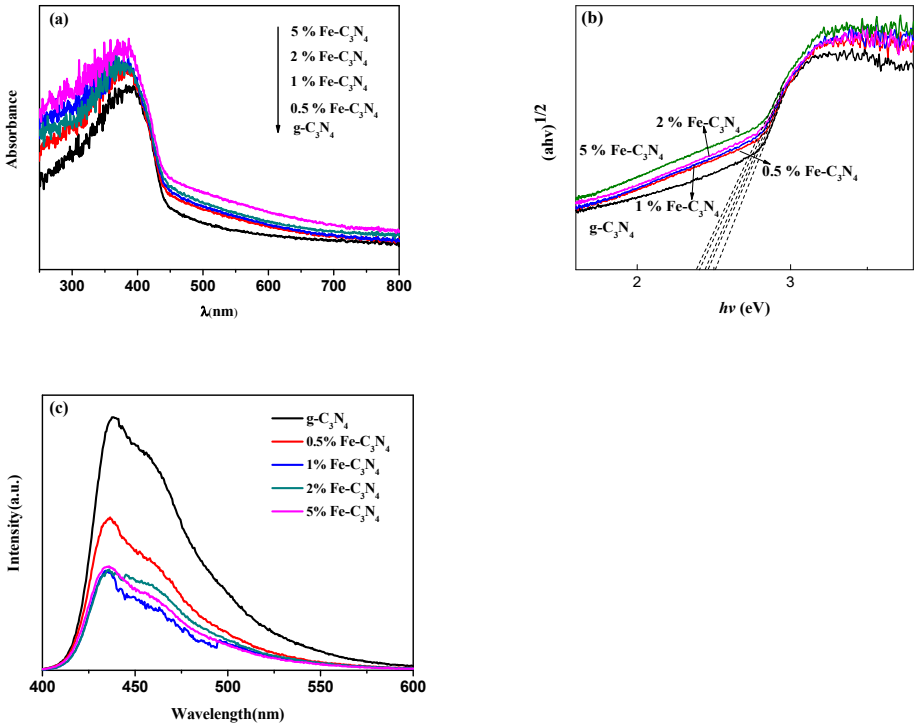


**Fig.3**. UV-vis diffuse reflectance spectra **(a)**, the Tauc's plot **(b)**, and photoluminescence emission spectra **(c)** of g-$C_3N_4$ and Fe-$C_3N_4$ samples.

### 3.2 Catalytic performance of Fe doped g-$C_3N_4$

From the results of XPS, synthesized Fe-$C_3N_4$ materials had large amounts of Fe-N sites. Therefore,

it was expected that Fe-$C_3N_4$ would show a good performance for removal of organic molecules in the photo-Fenton-like system. The cationic MB was chosen as a model pollutant for evaluating catalytic activity of synthesized materials. Experiments of MB oxidation were conducted without pH control (initial pH=6.86) and the results were shown in Fig.4(a). The degradation efficiency of MB by $H_2O_2$ in the dark, $H_2O_2$ under simulated sun-light irradiation, Fe-$C_3N_4$ in the dark, Fe-$C_3N_4$ under irradiation, and Fe-$C_3N_4$ assisting with $H_2O_2$ in the dark was 5.9%, 45.3%, 4.7%, 42.8% and 35.8%, respectively. Besides, the degradation efficiency of MB in g-$C_3N_4$, $H_2O_2$ and simulated sun-light irradiation system was 71.6%. Obviously, the Fe-$C_3N_4$ heterogeneous photo-Fenton-like system displayed an excellent performance towards MB degradation compared to other reaction systems and the degradation efficiency reached to 85.9%. From the results, it was inferred that the synergetic effect was formed between Fe-$C_3N_4$ and $H_2O_2$ under simulated sun light irradiation. The high removal efficiency of MB in Fe-$C_3N_4$ heterogeneous photo-Fenton-like system may be contributed from these reasons as follow: (1) The photocatalytic efficiency of g-$C_3N_4$ was improved by Fe doping. (2) The photo-generated electrons of Fe-$C_3N_4$ were captured by $H_2O_2$, and the separation of photo-generated electron and hole was enhanced. (2) The $H_2O_2$ was activated to generate ·OH by the photo-generated electron and $Fe^{3+}/Fe^{2+}$ cycle under light irradiation.

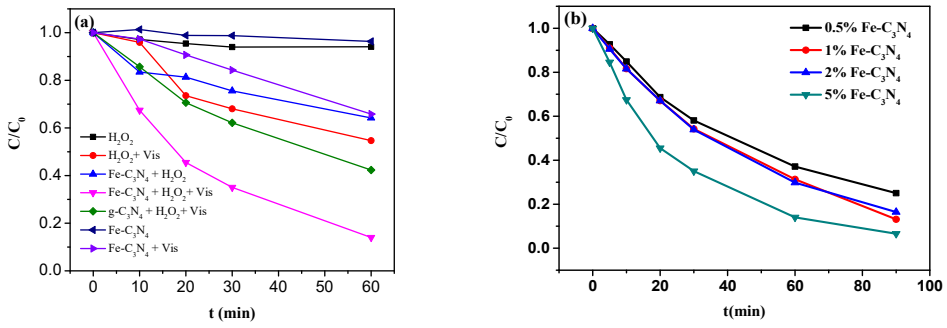

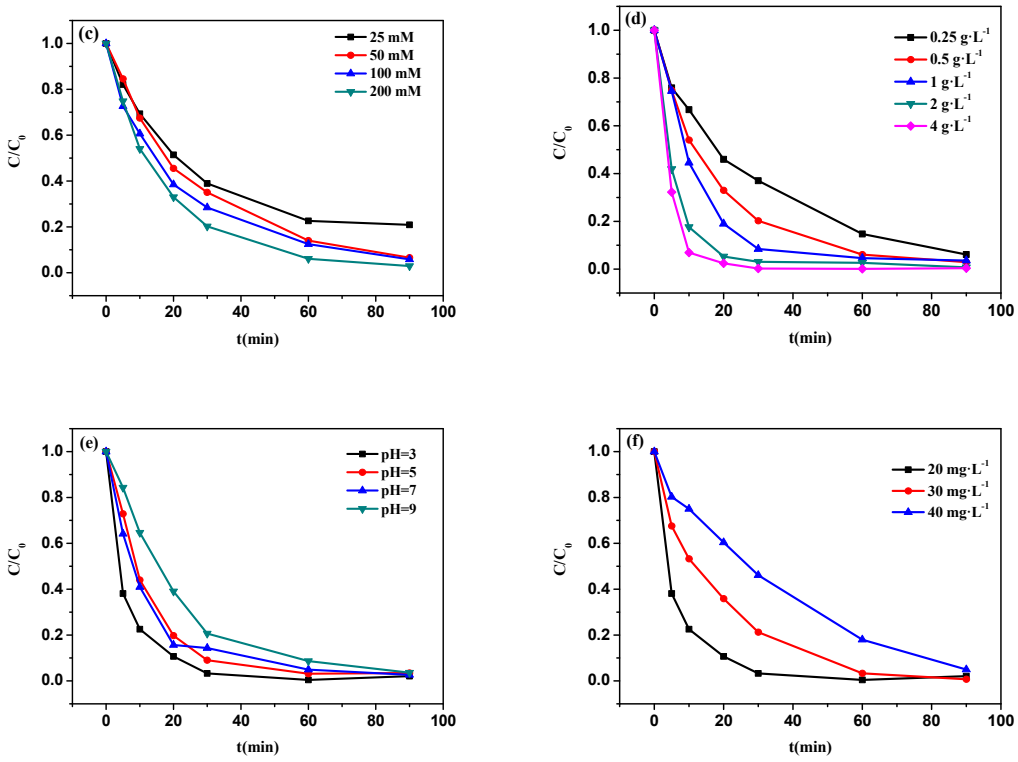


**Fig. 4**. Decolorization of MB under different system **(a)**, effect of Fe doped amounts **(b)**, effect of $H_2O_2$ concentration **(c)**, effect of catalyst dosage **(d)**, effect of pH **(e)**, effect of MB initial concentration **(f)**. Experimental condition: For **(a)**, [MB] = 20 mg·L$^{-1}$, [5 wt% Fe-$C_3N_4$] = 0.5 g·L$^{-1}$, [$H_2O_2$] = 50 mM, pH = 6.86. For **(b)**, [MB] = 20 mg·L$^{-1}$, [Fe-$C_3N_4$] = 0.5 g·L$^{-1}$, [$H_2O_2$] = 50 mM, pH = 6.86. For **(c)**, [MB] = 20 mg·L$^{-1}$, [5 wt% Fe-$C_3N_4$] = 0.5 g·L$^{-1}$, pH = 6.86. For **(d)**, [MB] = 20 mg·L$^{-1}$, [$H_2O_2$] = 200 mM, pH = 6.86. For **(e)**, [MB] = 20 mg·L$^{-1}$, [5 wt% Fe-$C_3N_4$] = 2 g·L$^{-1}$, [$H_2O_2$] = 200 mM. For **(f)**, [5 wt% Fe-$C_3N_4$] = 2 g·L$^{-1}$, [$H_2O_2$] = 200 mM, pH = 3.

### 3.3 Effect of reagent doses and pH on the degradation of MB

The effect of Fe doping amounts on the MB degradation were investigated in the range of 0.5-5 wt% and the result was shown in Fig.4(b). From the result, Fe doping amounts had an obviously promoted effect on the degradation of MB. With the increase of Fe doping amounts from 0.5 wt% to 5 wt%, the degradation efficiency of MB increased from 75% to 95%. This result demonstrated that the Fe doping amounts played a major role in degradation of MB and the Fe-N bond in the catalyst can activate the

237 $H_2O_2$ to produce hydroxyl radicals. With the content of $Fe^{3+}$ doping improving, the more ·OH was
238 generated in the system for degradation of MB.

239 The effect of $H_2O_2$ concentration was investigated in the range of 25 to 200 mM as shown in Fig.4(c).
240 The degraded performance of MB was obviously enhanced by increased the concentration of $H_2O_2$.
241 Degradation efficiency increased from 79.2% to 97.1% when the concentration of $H_2O_2$ increased from
242 25 to 200 mM. This result may be attributed to an increase in the rate of ·OH produced by Fe-$C_3N_4$ and
243 $H_2O_2$ under simulation sunlight irradiation. However, the degradation efficiency had little change when
244 the dosage of $H_2O_2$ from 100 to 200 mM. Therefore, there was no requirement to continue increasing the
245 concentration of $H_2O_2$.

246 To investigate the influence of the dosage of Fe-$C_3N_4$, five different values were tested as shown in
247 Fig.4(d). Apparently, the increase of Fe-$C_3N_4$ dosage from 0.25 to 2 $g \cdot L^{-1}$ had a promoted effect on the
248 degradation of MB. The degradation efficiency increased significantly from 62.99% to 96.95% within
249 30 minutes. The amounts of active sites in the Fe-$C_3N_4$ heterogenous photo-Fenton-like system affected
250 the degradation rate of MB, and the degradation rate was limited to low Fe-$C_3N_4$ dosage by reason of not
251 enough active sites. However, with the increase of Fe-$C_3N_4$ dosage from 2 to 4 $g \cdot L^{-1}$, the MB degradation
252 curves showed very similar profiles within 90 minutes. The photocatalytic degradation performance of
253 MB was determined by the amounts of active sites on the catalyst and the penetration of simulated solar
254 irradiation. With increasing the dosage of Fe-$C_3N_4$, the number of active sites would increase and more
255 photoelectron could be generated resulted to more ·OH produced from $H_2O_2$. However, the light
256 reflectance and shielding effect would occur by the excess Fe-$C_3N_4$ dosages. Therefore, the degradation
257 efficiency of MB had no obvious change with increase of Fe-$C_3N_4$ from 2 to 4 $g \cdot L^{-1}$.

258 The effect of pH within ranges 3-9 on the MB degradation in the Fe-$C_3N_4$ heterogeneous photo-

Fenton-like system was investigated. As shown in Fig. 4(e), the catalyst remains highly active towards MB degradation over an initial broad pH range from 3 to 9. When pH increased from 3 to 9, the efficiency of MB degradation decreased slightly. Interestingly, at first 30 min, the heterogeneous photo-Fenton-like system degradation efficiency at pH=3, 5, 7 and 9 was 97%, 91%, 85% and 79%, respectively. This phenomenon was attributed to different Fe-N ligands formed in the system. At acidic condition, the produced Fe-N ligands was more conducive to activate $H_2O_2$ compared to the ligands formed under alkaline conditions. Besides, the $H_2O_2$ can be consumed and decomposed to $H_2O$ and $O_2$ under alkaline conditions. In general, at 90 min, all the decolorization ratio of MB with pH rising from 3 to 9 was more than 90%. Hence, Fe-$C_3N_4$ heterogeneous photo-Fenton-like system showed a wide pH range compared to the conventional Fenton system.

The effect of initial MB concentration on the degradation was examined in the range of 20 to 40 $mg \cdot L^{-1}$. As shown in Fig. 4(f), the degradation efficiency of MB within 90 min reached to almost 100% with increasing MB concentration from 20 to 40 $mg \cdot L^{-1}$. However, at first 30 min, the degradation efficiency decreased from 96.7% to 53.9% with the increase of MB concentration from 20 to 40 $mg \cdot L^{-1}$. This result was attributed to the amounts of the active species. With the increase of initial MB concentration, the more active species were required for the degradation of MB. However, the active species in the system were theoretically constant at the fixed Fe-$C_3N_4$ dosage, $H_2O_2$ concentration and light intensity. Thus, the active species were inadequate for higher MB concentration.

### 3.4 Effect of inorganic ions on the degradation of MB

Various inorganic ions may co-exist with dye waste water. Thus, to examine the effect of co-existing ions on the MB degradation is very important and benefit of realistic dye treatment process. Previous studies have confirmed that the presence of some inorganic ions in the photocatalytic system can affect

the degradation of MB [36-39]. To investigate the effect of the co-existing various inorganic ions on the MB degradation, photocatalytic degradation of MB was conducted with six typical inorganic ions of nitrate ($NO_3^-$), chloride ($Cl^-$), bicarbonate ions ($HCO_3^-$), aluminum ions ($Al^{3+}$), magnesium ions ($Mg^{2+}$) and calcium ions ($Ca^{2+}$). Considering that natural water does not contain buffer solution and the introduction of buffer solution will make the system more complicated, the influence of inorganic ions was not investigated in buffer solution.

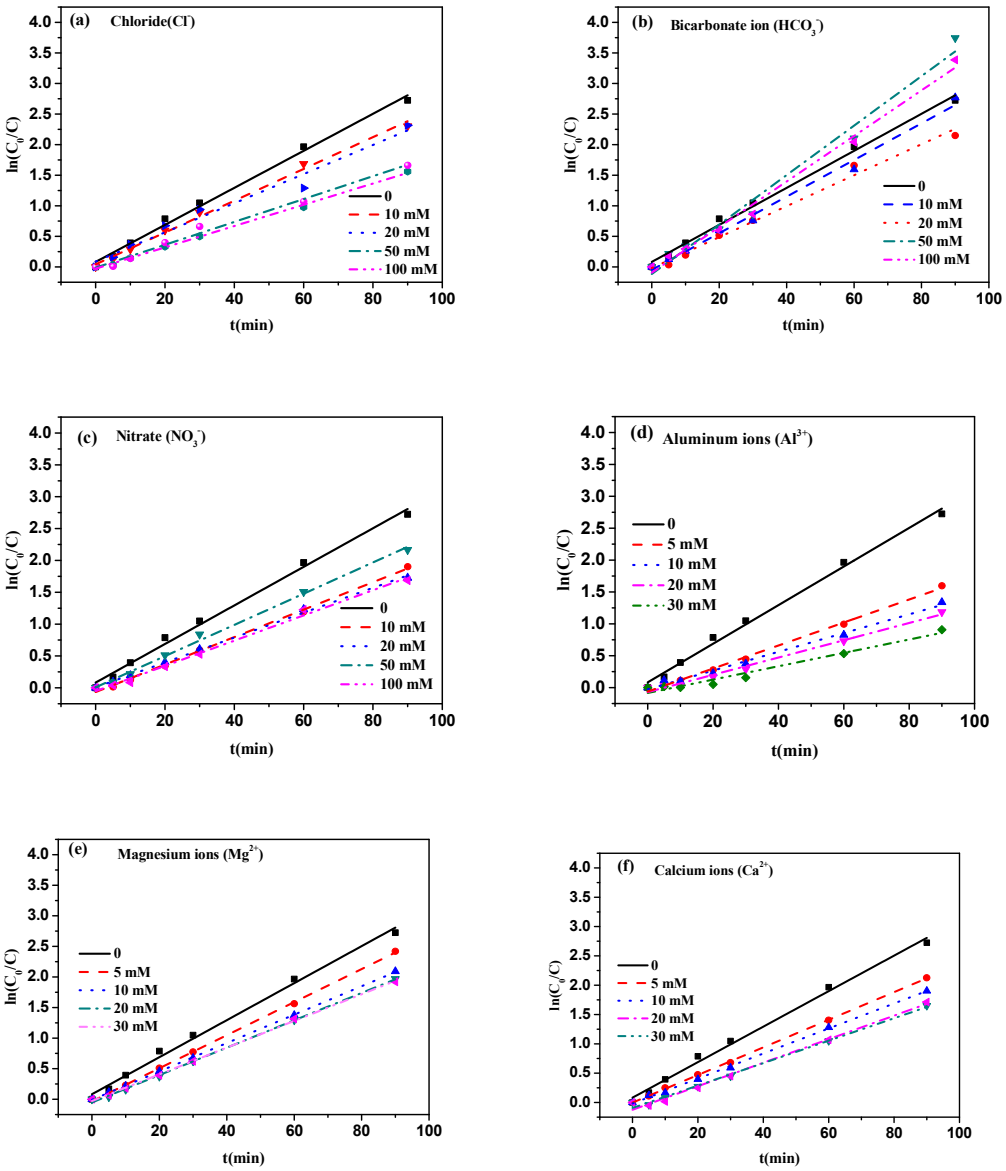


**Fig. 5**. Effect of inorganic anions and cations on MB degradation under simulated solar light irradiation **(a-e)**. Experimental condition :[MB] = 20 mg·$L^{-1}$, [5 wt% Fe-$C_3N_4$] = 0.5 g·$L^{-1}$, no pH adjustment and

original pH=6.86, [$Cl^-$], [$HCO_3^-$] and [$NO_3^-$] = 10, 20, 50, 100 mM, [$Al^{3+}$], [$Mg^{2+}$] and [$Ca^{2+}$] =5, 10, 20, 30 mM.

Effect of $Cl^-$ on the degradation of MB in the Fe-$C_3N_4$ heterogenous photo-Fenton-like system was investigated under different $Cl^-$ concentrations from 0 to 100 mM. Fig.5(a) showed that efficient degradation of MB was inhibited by the $Cl^-$. Adding concentrations of $Cl^-$ obviously decreased the *k* values of MB degradation rate (Fig. 5(a) and Table S1). The *k* values of MB degradation rate decreased from 0.0302 to 0.0187 $min^{-1}$ with increasing the concentration of $Cl^-$ from 0 to 100 mM. This phenomenon could be attributed to the reaction of ·OH with $Cl^-$ generated $ClOH^{\cdot -}$ (Eq. (3)) that the reactivity is not as reactive •OH. In this circumstance, $Cl^-$ act as ·OH scavenger, inhibiting the MB degradation [43].

Fig.5(b) showed that the effect of $HCO_3^-$ on MB degradation in the Fe-$C_3N_4$ heterogenous photo-Fenton-like system. With the increase of $HCO_3^-$ concentrations from 0 to 20 mM, the *k* values of MB degradation rate decreased from 0.0303 to 0.0299 $min^{-1}$ (Table S1). However, the *k* values improved with the further increase of $HCO_3^-$ concentration. It has been found that $HCO_3^-$ could react with •OH to produce the carbonate radical ($CO_3^{\cdot -}$) (Eq. (4)). Meanwhile, the ionization reactions of carbonic acid to reach the equilibration would occur (Eq. (5)-(8)) [43], and the concentration of $HCO_3^-$ could influence the pH of the reaction system. Therefore, the effect of different $HCO_3^-$ concentration on the degradation of MB can be explained by these reasons. (1) At a low $HCO_3^-$ concentration (10, 20 mM), the $HCO_3^-$ may mostly play the role of ·OH scavenger and the produced $CO_3^{\cdot -}$ would not involve in the degradation of MB. The degradation rate of MB decreased due to ·OH scavenging. (2) At a high $HCO_3^-$ concentration (50, 100 mM), the degradation rate increased because the abundant of $CO_3^{\cdot -}$ was produced and participated in the MB degradation. Besides, with the increase of the $HCO_3^-$ concentration, the changed

315 pH of reaction system from neutral to alkaline could result in negative charge Fe-g-$C_3N_4$, and more MB
316 molecule could be contacted and degraded.

317 As for $NO_3^-$, Fig.5(c) showed the MB degradation rate *k* values at different concentration from 0 to
318 100 mM. The $NO_3^-$ showed an inhibition effect in the Fe-$C_3N_4$ heterogenous photo-Fenton system. With
319 the increase of $NO_3^-$ concentration from 0 to 20 mM, the *k* values of MB degradation rate decreased from
320 0.0303 to 0.0195 $min^{-1}$ (Table.S1). This result might be attributed to the reaction between ·OH and $NO_3^-$.
321 The ·OH could react with $NO_3^-$ to produce the nitrate radical ($NO_3^{-}$·) (Eq. (9)) that the redox ability is
322 weaker than ·OH [43]. However, when the $NO_3^-$ concentration was further increased from 20 to 50 mM,
323 the *k* values of MB degradation rate increased from 0.0195 to 0.0245 $min^{-1}$. When the concentrations of
324 $NO_3^-$ were more than 20 mM, the *k* values of MB degradation were improved. This phenomenon might
325 be due to the formation of ·OH under simulated solar irradiation (Eq. (10)) [43]. Interestingly, further
326 increased of $NO_3^-$ concentration to 100 mM, the *k* values of MB degradation rate decreased to 0.0198
327 $min^{-1}$. When the concentration of the $NO_3^-$ further increased, more ·OH was consumed by $NO_3^-$ rather
328 than produced. Therefore, MB removal efficiency exhibited an irregularly inhibition effects by $NO_3^-$.

329 Influence of inorganic cations on the degradation of MB in the Fe-$C_3N_4$ heterogenous photo-Fenton
330 system was investigated under various concentrations from 0 to 30 mM. Inorganic cations including $Al^{3+}$,
331 $Mg^{2+}$, and $Ca^{2+}$ exhibited an obviously inhibited effect on the degradation of MB, as shown in Fig. 5((d)-
332 (f)) and Table.S2. Among three kind of cations, the $Al^{3+}$ ions showed a maximum negative effect on the
333 *k* values of MB degradation rate and the *k* value decreased from 0.0303 to 0.0105 $min^{-1}$ with increasing
334 concentration of $Al^{3+}$ from 5 to 30 mM. Compared with the $Mg^{2+}$ and $Ca^{2+}$, the *k* value decreased 2.88
335 times with 30 mM $Al^{3+}$ addition. This result could be explained by that $Al^{3+}$, $Mg^{2+}$ and $Ca^{2+}$ were absorbed
336 onto Fe-$C_3N_4$ surface. At the same time, the accompanying shielding effect, reduction of active sites and

the penetration of light irradiation caused the low photocatalytic efficiency [38, 40-43].

$$\bullet OH + Cl^- \rightarrow ClOH^{\cdot -} \quad (3)$$

$$\bullet OH + HCO_3^- \rightarrow CO_3^{\cdot -} + H_2O \quad (4)$$

$$H_2CO_3 \leftrightarrow H^+ + HCO_3^- , \ pka_1 = 6.38 \quad (5)$$

$$HCO_3^- \leftrightarrow H^+ + CO_3^{2-}, \ pka_2 = 10.38 \quad (6)$$

$$CO_3^{2-} + H_2O \rightarrow OH^- + HCO_3^- \quad (7)$$

$$HCO_3^- + H_2O \rightarrow OH^- + H_2CO_3 \quad (8)$$

$$\bullet OH + NO_3^- \rightarrow NO_3^{\cdot -} \quad (9)$$

$$NO_3^- + H_2O + hv \rightarrow NO_2^{\cdot} + OH^- + \cdot OH \quad (10)$$

**3.5 Stability of Fe-$C_3N_4$ catalyst**

With reference to the practical application of Fe-$C_3N_4$ heterogeneous photo-Fenton-like system, the stability of the catalyst was examined. As the result shown in Fig. 6(a), MB degradation efficiency was still more than 90% within 90 min after three cycles. The residual amount of iron ion in the solution after the reaction was measured by an atomic absorption spectrophotometer (AA-700, Shimadzu International Trading Co., Ltd.) and the concentration of iron ion was 0.4781 mg·$L^{-1}$. The concentration of leaching Fe content was lower than the limitation in drinking-water in EU and US (< 2 ppm) [32, 44, 45]. In addition, the XRD result of the used catalyst as shown in Fig. 6(b) and the XRD patterns of Fe-$C_3N_4$ had no obviously change. These results demonstrated that Fe-$C_3N_4$ has a good reusability and stability.

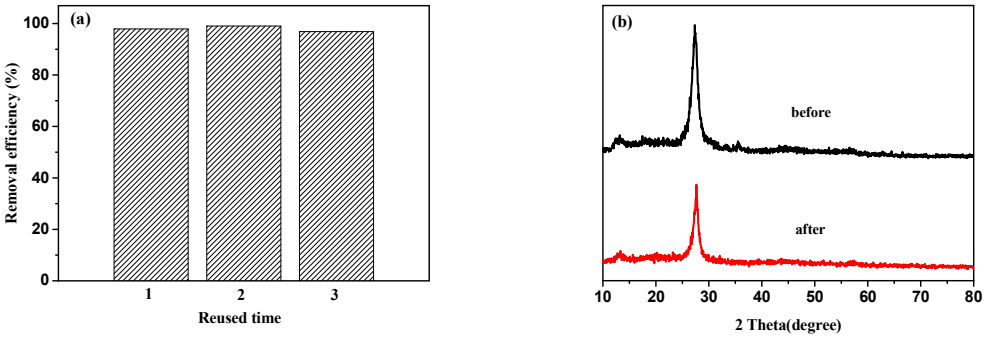


**Fig. 6**. The degradation efficiency of MB under recycling experiment **(a)** and XRD survey of Fe-$C_3N_4$ before and after decolorization of MB in the Fe-$C_3N_4$ heterogenous photo-Fenton-like system **(b)**. Experimental condition: For **(a)** and **(b)**, [MB] = 20 mg·$L^{-1}$, [5 wt% Fe-$C_3N_4$] = 2 g·$L^{-1}$, [$H_2O_2$] = 200 mM, pH = 3.

### 3.6 Degradation mechanism of Fe-$C_3N_4$ heterogeneous photo-Fenton-like system

It was considered that MB molecule was broken and degraded into smaller molecules in the Fe-$C_3N_4$ heterogenous photo-Fenton-like system. To demonstrate this hypothesis, the UV-vis adsorption spectra was conducted as shown in Fig. 7(a). The result showed the absorption spectral variation of MB with irradiation time. Two main absorbance peaks were observed at 665 and 290 nm, respectively. The peak at 665 nm was attributed to the chromophore (-C=S) of MB and the peak at 290 nm was attributed to the unsaturated conjugate aromatic rings [24, 46, 47]. It was obvious that the adsorption peaks at 665 and 290 nm decreased significantly with irradiation time, suggesting that the conjugate structure of MB was destroyed and the aromatic rings of MB was degraded in the system. Besides, with the reaction time increasing, the position of maximum absorbance peak at 665 nm without shift. Related research showed that the peak at 665 nm of MB blue shifted was related to occurring of N-demethylation intermediates of MB [24]. Thus, we inferred that the initial step of MB degradation in the Fe-$C_3N_4$ heterogeneous photo-Fenton system may not involve N-demethylation. To investigated the reactive species of MB degradation in the system, quenching experiments by TBA, KI and 1,4-benzoquinone were conducted [48]. In this section, 2 mM TBA, 2 mM p-benzoquinone and 2 mM KI were used as the quenchers of ·OH, $\cdot O_2^-$ and $h^+$, respectively. As shown in Fig. 7(b), at first 30 min, the MB degradation efficiency decreased from 96.7% to 93.2%, 86.1%, and 75.3% after adding 1,4-benzoquinone, KI, and TBA, respectively. It was found that 1,4-benzoquinone had little effect on MB removal in this system and TBA showed

significantly inhibited effect on MB degradation. The result implied the fact that •OH was a major active species in the system. When 1,4-benzoquinone was added in the reaction system, the degradation efficiency of MB was affected but without decreasing within 30 min, and was nearly similar to the performance of control experiment. This result demonstrated that $O_2^{-}\cdot$ rarely or not formed during this reaction system. However, the MB degradation efficiency has an enhancement when 1,4-benzoquinone was added into catalytic system at the first 20 min. This phenomenon may be due to the activation of $H_2O_2$ by 1,4-benzoquinone. Several literatures have reported that peroxydisulfate and $H_2O_2$ can be activated by organic quinones. For instance, Zhou et al found that peroxymonosulfate could be activated by benzoquinone [49]. Fang et al reported that 1,4-benzoquinone, 2-methyl-1,4-benzoquinone or 2-chloro-1,4-benzoquinone could enhance the degraded efficiency of 2,4,4′-trichlorobiphenyl by peroxydisulfate [50]. Zhu et al reported that halogenated quinones could activate $H_2O_2$ to produce •OH [51]. Besides, Chen et al investigated the degradation of tetracycline by $H_2O_2$ alone, and similar phenomenon was found that the tetracycline degradation efficiency has an enhancement when benzoquinone was added into catalytic system at the first 45 min [52].

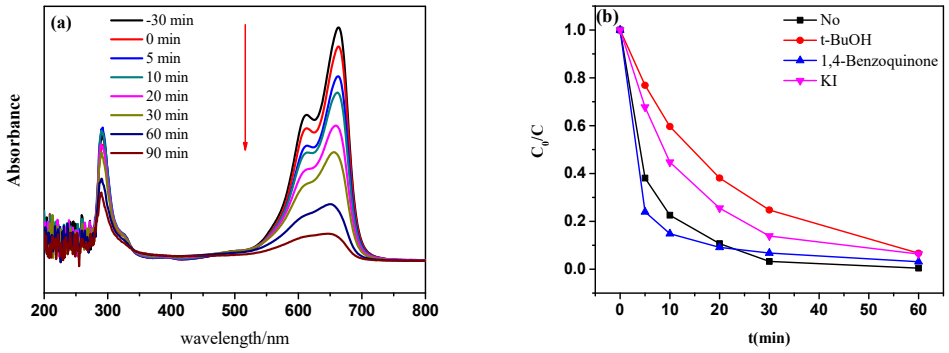


**Fig. 7**. Temporal evolution of the UV–vis spectra during decolorization of MB in the Fe-$C_3N_4$ heterogenous photo-Fenton-like system **(a)** and influences of radical scavengers on decolorization of MB **(b)**. Experimental condition: For **(a)**, [MB] = 20 mg·$L^{-1}$, [5 wt% Fe-$C_3N_4$] = 0.5 g·$L^{-1}$, [$H_2O_2$] = 50 mM, pH= 3. For **(b)**, [MB] = 20 mg·$L^{-1}$, [5 wt% Fe-$C_3N_4$] = 2 g·$L^{-1}$, [$H_2O_2$] = 200 mM, [t-BuOH] = 2 mM, [1,4-Benzoquinone] = 2 mM, [KI] = 2 mM, pH = 3.

For degradation pathway analysis, the intermediate products resulting from MB degradation at 60 min were analyzed by LC-MS. According to the results, nine main intermediate product ions at m/z

305.16, m/z 301.17, m/z 143.09, m/z 135.12, m/z 130.16, m/z 109.10, m/z 95.09, m/z 93.04 and m/z 75.03 were detected at different retention time, which probably corresponded to $C_{16}H_{23}N_3SO$, $C_{16}H_{19}N_3SO$, $C_6H_6O_4$, $C_7H_5NS$, $C_6H_{13}NO_2$, $C_6H_7NO$, $C_6H_6O$, $C_6H_7N$ and $C_2H_2O_3$, respectively (Table. S3). It was confirmed that the benzene ring of MB could be hydroxylated by •OH in the previous work [24, 53, 54]. However, we did not observe corresponding intense fragments in this study. Thus, the •OH may played a role in aromatic ring opening and oxidation. Meanwhile, based on intermediates from previous work [55-62], the possible pathway of MB degradation by Fe-$C_3N_4$ heterogenous photo-Fenton-like system was proposed in Fig. S3. The Cl in the MB molecule was firstly ionized, after that C-$N^+$=C and C-$S^+$-C were destroyed. Then, -N=$(CH_3)_2$ groups were also degraded and induced the breakup of the aromatic rings. In the process, produced intermediates such as DL-Norleucine, phenol and Benzothiadiazole, which partly were further mineralized to carbon dioxide, water and inorganic anions ($SO_4^{2-}$, $NH_4^+$ and $NO_3^-$).

The XPS results showed the Fe(III)-N was the main active sites for the photo-Fenton-like reaction. By combining XPS results and previous works [32, 63, 64], we proposed a possible mechanism of this catalytic system(Fig.8). There were two pathways to generate ·OH (Eqs.(11)-(13)). (1) Fe-$C_3N_4$ was excited to generate electrons and holes under simulated sunlight. The Fe(III)-N accepted electrons transformed to Fe(II)-N. The Fe(II)-N and $H_2O_2$ combined to generated Fe(III)-N and ·OH by electron transfer. At the same time, a series of chain reactions were initiated, including the formation of redox cycles of ·OH and Fe(III)/Fe(II). (2) $H_2O_2$ decomposed to ·OH under simulated sunlight. Theoretically, the VB of g-$C_3N_4$ was +1.57 V and the redox potentials of $\cdot OH/OH^-$ was +1.99 V. Thus, ·OH cannot generated from VB holes in the g-$C_3N_4$. In the Fe-$C_3N_4$ heterogenous photo-Fenton-like system, MB was absorbed in the surface of Fe-$C_3N_4$ firstly. Then, MB attacked by ·OH and transformed to small molecule

organics, inorganic ions, $CO_2$ and $H_2O$.

$$Fe(III)\text{-}N + e^- \rightarrow Fe(II)\text{-}N \quad (11)$$

$$Fe(II)\text{-}N + H_2O_2 \rightarrow \bullet OH + Fe(III)\text{-}N \quad (12)$$

$$H_2O_2 + e^- \rightarrow \bullet OH + OH^- \quad (13)$$

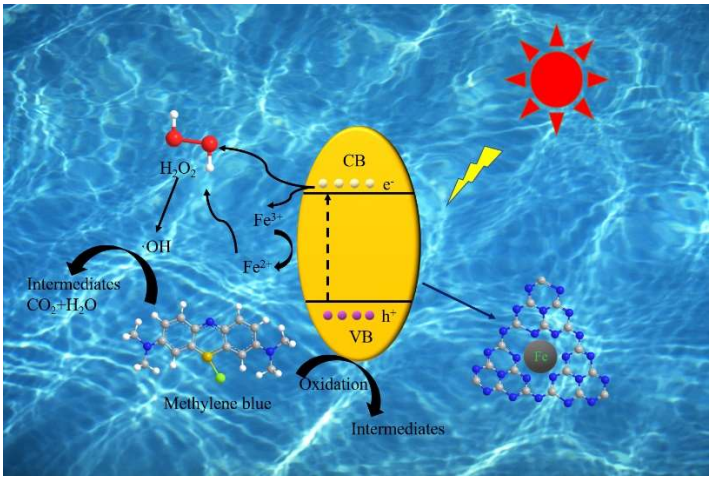


**Fig.8**. Schematic diagram of Fe-$C_3N_4$ catalyzed heterogeneous photo-Fenton-like reaction.

## 4. Conclusions

In this study, Fe-$C_3N_4$ was fabricated and applied in the heterogeneous photo-Fenton-like system. Fe-$C_3N_4$ exhibited superb performance for degradation of MB in the pH range of 3-9. The effect of various inorganic ions on the degradation of MB was studied where $Cl^-$ and $NO_3^-$ inhibited the degradation of MB, $HCO_3^-$ exhibited a dual effect. The presence of cations ($Al^{3+}$, $Mg^{2+}$, $Ca^{2+}$) inhibits the degradation of MB, and the order of the inhibitory effect was: $Al^{3+} > Ca^{2+} > Mg^{2+}$. The catalyst cycle experiment illustrated that Fe-$C_3N_4$ was highly stable with consistently high degradation of MB. According to the quenching experiment, dominated activated species was • OH. In short, this photo assisted heterogeneous Fenton-like process had a highly efficient removal of MB while overcame the common questions in conventional Fenton system.

## Conflicts of interest

There are no conflicts to declare.

## Acknowledgements

This study was funded by National Natural Science Foundation of China (grant number 21367003), Guangxi Major Project Science and Technology (grant number AA17129001) and Guangxi Key Laboratory of Clean Pulp & Papermaking and Pollution Control Open Foundation (grant number KF201724).

## Notes and references

1. D. B. Miklos, C. Remy, M. Jekel, K. G. Linden, J. E. Drewes and U. Hübner, *Water Research*, 2018, **139**, 118-131.
2. T. Guo, K. Wang, G. Zhang and X. Wu, *Applied Surface Science*, 2019, **469**, 331-339.
3. Z. Xiong, Z. Wang, M. Muthu and Y. Zhang, *Journal of Hazardous Materials*, 2019, **373**, 565-571.
4. S. Yang, P. Wu, J. Liu, M. Chen, Z. Ahmed and N. Zhu, *Chemical Engineering Journal*, 2018, **350**, 484-495.
5. J. Liu, P. Wu, S. Yang, S. Rehman, Z. Ahmed, N. Zhu, Z. Dang and Z. Liu, *Applied Catalysis B: Environmental*, 2020, **261**, 118232.
6. C. Cai, Z. Zhang, J. Liu, N. Shan, H. Zhang and D. D. Dionysiou, *Appl. Catal. B-Environ.*, 2016, **182**, 456-468.
7. X. Y. Li, Y. H. Pi, L. Q. Wu, Q. B. Xia, J. L. Wu, Z. Li and J. Xiao, *Appl. Catal. B-Environ.*, 2017, **202**, 653-663.
8. J. Fu, J. Yu, C. Jiang and B. Cheng, *Advanced Energy Materials*, 2018, **8**, 1701503.
9. Z. Sun, H. Wang, Z. Wu and L. Wang, *Catalysis Today*, 2018, **300**, 160-172.
10. X. Zhang, X. Zhang, J. Li, J. Sun, J. Bian, J. Wang, Y. Qu, R. Yan, C. Qin and L. Jing, *Applied Catalysis B: Environmental*, 2018, **237**, 50-58.
11. A. Nikokavoura and C. Trapalis, *Applied Surface Science*, 2018, **430**, 18-52.
12. Y. Yu, W. Yan, X. Wang, P. Li, W. Gao, H. Zou, S. Wu and K. Ding, *Adv. Mater.*, 2018, **30**, 1705060.
13. X. Ma, Y. Lv, J. Xu, Y. Liu, R. Zhang and Y. Zhu, *The Journal of Physical Chemistry C*, 2012, **116**, 23485-23493.
14. J. Jiang, S. Cao, C. Hu and C. Chen, *Chinese Journal of Catalysis*, 2017, **38**, 1981-1989.
15. W. Yan, L. Yan and C. Jing, *Applied Catalysis B: Environmental*, 2019, **244**, 475-485.
16. Y. Wang, S. Zhao, Y. Zhang, W. Chen, S. Yuan, Y. Zhou and Z. Huang, *Applied Surface Science*, 2019, **463**, 1-8.
17. S. Hu, L. Ma, J. You, F. Li, Z. Fan, G. Lu, D. Liu and J. Gui, *Applied Surface Science*, 2014, **311**, 164-171.
18. Q. Liu, T. Chen, Y. Guo, Z. Zhang and X. Fang, *Applied Catalysis B: Environmental*, 2017, **205**, 173-181.

19. J. Gao, Y. Wang, S. Zhou, W. Lin and Y. Kong, *ChemCatChem*, 2017, **9**, 1708-1715.
20. W.-D. Oh, V. W. C. Chang, Z.-T. Hu, R. Goei and T.-T. Lim, *Chemical Engineering Journal*, 2017, **323**, 260-269.
21. X. Chen, J. Zhang, X. Fu, M. Antonietti and X. Wang, *Journal of the American Chemical Society*, 2009, **131**, 11658-11659.
22. X. Song, H. Tao, L. Chen and Y. Sun, *Materials Letters*, 2014, **116**, 265-267.
23. S. Hu, R. Jin, G. Lu, D. Liu and J. Gui, *Rsc Advances*, 2014, **4**, 24863-24869.
24. Y. Liu, W. Jin, Y. Zhao, G. Zhang and W. Zhang, *Applied Catalysis B: Environmental*, 2017, **206**, 642-652.
25. S. Yan, Z. Li and Z. Zou, *Langmuir*, 2009, **25**, 10397-10401.
26. H. Li, C. Shan and B. Pan, *Environmental Science & Technology*, 2018, **52**, 2197-2205.
27. K. Wang, Q. Li, B. Liu, B. Cheng, W. Ho and J. Yu, *Applied Catalysis B: Environmental*, 2015, **176-177**, 44-52.
28. Y. Cui, Z. Ding, P. Liu, M. Antonietti, X. Fu and X. Wang, *Phys. Chem. Chem. Phys.*, 2012, **14**, 1455-1462.
29. S. Hu, X. Chen, Q. Li, F. Li, Z. Fan, H. Wang, Y. Wang, B. Zheng and G. Wu, *Applied Catalysis B: Environmental*, 2017, **201**, 58-69.
30. X. Du, X. Yi, P. Wang, J. Deng and C.-c. Wang, *Chinese Journal of Catalysis*, 2019, **40**, 70-79.
31. A. Mirzaei, Z. Chen, F. Haghighat and L. Yerushalmi, *Applied Catalysis B: Environmental*, 2019, **242**, 337-348.
32. J. Ma, Q. Yang, Y. Wen and W. Liu, *Applied catalysis B: environmental*, 2017, **201**, 232-240.
33. M. Chen, P. Wu, L. Yu, S. Liu, B. Ruan, H. Hu, N. Zhu and Z. Lin, *Journal of environmental management*, 2017, **192**, 31-38.
34. X. Wang, X. Chen, A. Thomas, X. Fu and M. Antonietti, *Adv. Mater.*, 2009, **21**, 1609-1612.
35. W.-J. Ong, L.-L. Tan, Y. H. Ng, S.-T. Yong and S.-P. Chai, *Chemical reviews*, 2016, **116**, 7159-7329.
36. C. Guillard, H. Lachheb, A. Houas, M. Ksibi, E. Elaloui and J.-M. Herrmann, *Journal of Photochemistry and Photobiology A: Chemistry*, 2003, **158**, 27-36.
37. A.-G. Rincón and C. Pulgarin, *Applied Catalysis B: Environmental*, 2004, **51**, 283-302.
38. I. K. Konstantinou and T. A. Albanis, *Applied Catalysis B: Environmental*, 2004, **49**, 1-14.
39. C. Hu, J. C. Yu, Z. Hao and P. K. Wong, *Applied Catalysis B: Environmental*, 2003, **46**, 35-47.
40. X. Gao, X. Zhang, Y. Wang, S. Peng, B. Yue and C. Fan, *Chemical Engineering Journal*, 2015, **273**, 156-165.
41. S. Liu, P. Wu, M. Chen, L. Yu, C. Kang, N. Zhu and Z. Dang, *Environmental Pollution*, 2017, **228**, 277-286.
42. C. Liu, P. Wu, Y. Zhu and L. Tran, *Chemosphere*, 2016, **144**, 1026-1032.
43. L. Chen, P. Wu, M. Chen, X. Lai, Z. Ahmed, N. Zhu, Z. Dang, Y. Bi and T. Liu, *Applied Clay Science*, 2018, **159**, 74-82.
44. X.-j. Yang, X.-m. Xu, J. Xu and Y.-f. Han, *Journal of the American Chemical Society*, 2013, **135**, 16058-16061.
45. X. Li, X. Liu, L. Xu, Y. Wen, J. Ma and Z. Wu, *Applied Catalysis B: Environmental*, 2015, **165**, 79-86.
46. Y. Li and F.-S. Zhang, *Chemical Engineering Journal*, 2010, **158**, 148-153.

47. B. Zhou, X. Zhao, H. Liu, J. Qu and C. P. Huang, *Applied Catalysis B: Environmental*, 2010, **99**, 214-221.
48. J. Wang, Y. Xia, H. Zhao, G. Wang, L. Xiang, J. Xu and S. Komarneni, *Applied Catalysis B: Environmental*, 2017, **206**, 406-416.
49. Y. Zhou, J. Jiang, Y. Gao, J. Ma, S.-Y. Pang, J. Li, X.-T. Lu and L.-P. Yuan, *Environmental science & technology*, 2015, **49**, 12941-12950.
50. G. Fang, J. Gao, D. D. Dionysiou, C. Liu and D. Zhou, *Environmental science & technology*, 2013, **47**, 4605-4611.
51. B.-Z. Zhu, H.-T. Zhao, B. Kalyanaraman and B. Frei, *Free Radical Biology and Medicine*, 2002, **32**, 465-473.
52. Y.-Y. Chen, Y.-L. Ma, J. Yang, L.-Q. Wang, J.-M. Lv and C.-J. Ren, *Chemical Engineering Journal*, 2017, **307**, 15-23.
53. L. C. A. Oliveira, M. Gonçalves, M. C. Guerreiro, T. C. Ramalho, J. D. Fabris, M. C. Pereira and K. Sapag, *Applied Catalysis A: General*, 2007, **316**, 117-124.
54. H. A. Bicalho, J. L. Lopez, I. Binatti, P. F. R. Batista, J. D. Ardisson, R. R. Resende and E. Lorençon, *Molecular Catalysis*, 2017, **435**, 156-165.
55. S. Xia, L. Zhang, G. Pan, P. Qian and Z. Ni, *Phys. Chem. Chem. Phys.*, 2015, **17**, 5345-5351.
56. M. A. Rauf, M. A. Meetani, A. Khaleel and A. Ahmed, *Chemical Engineering Journal*, 2010, **157**, 373-378.
57. A. Houas, H. Lachheb, M. Ksibi, E. Elaloui, C. Guillard and J.-M. Herrmann, *Applied Catalysis B: Environmental*, 2001, **31**, 145-157.
58. H. Huang, D. Y. C. Leung, P. C. W. Kwong, J. Xiong and L. Zhang, *Catalysis Today*, 2013, **201**, 189-194.
59. A. Xu, X. Li, H. Xiong and G. Yin, *Chemosphere*, 2011, **82**, 1190-1195.
60. P. V. Bakre, P. S. Volvoikar, A. A. Vernekar and S. G. Tilve, *Journal of Colloid and Interface Science*, 2016, **474**, 58-67.
61. K. Yu, S. Yang, C. Liu, H. Chen, H. Li, C. Sun and S. A. Boyd, *Environmental Science & Technology*, 2012, **46**, 7318-7326.
62. Q. Wang, S. L. Tian and P. Ning, *Industrial & Engineering Chemistry Research*, 2014, **53**, 643-649.
63. J. Hu, P. Zhang, W. An, L. Liu, Y. Liang and W. Cui, *Applied Catalysis B: Environmental*, 2019, **245**, 130-142.
64. X. Qian, Y. Wu, M. Kan, M. Fang, D. Yue, J. Zeng and Y. Zhao, *Applied Catalysis B: Environmental*, 2018, **237**, 513-520.